Applied Physics Letters

Thermo-responsive mechano-optical plasmonic nano-antenna

Cite as: Appl. Phys. Lett. **109**, 013109 (2016); https://doi.org/10.1063/1.4954907
Submitted: 12 April 2016 • Accepted: 15 June 2016 • Published Online: 08 July 2016

Yunbo Liu, Younggeun Park and Somin Eunice Lee

Thermo-responsive mechano-optical plasmonic nano-antenna

Yunbo Liu,[1,2] Younggeun Park,[3] and Somin Eunice Lee[1,2,4,5,a)]
[1]*Department of Electrical and Computer Engineering, University of Michigan, Ann Arbor, Michigan 48109, USA*
[2]*Biointerfaces Institute, University of Michigan, Ann Arbor, Michigan 48109, USA*
[3]*Department of Mechanical Engineering, University of Michigan, Ann Arbor, Michigan 48109, USA*
[4]*Department of Biomedical Engineering, University of Michigan, Ann Arbor, Michigan 48109, USA*
[5]*Applied Physics Program, University of Michigan, Ann Arbor, Michigan 48109, USA*

(Received 12 April 2016; accepted 15 June 2016; published online 8 July 2016)

We propose and theoretically demonstrate a mechano-optical nano-antenna over a broad temperature range. We show that there is a tunable, temperature-dependent plasmonic resonance associated with the nano-antenna geometry. We also theoretically demonstrate a matching condition for mechanical properties that is essential for maximizing thermal expansion differences across a broad temperature range. We expect that mechano-optical nano-antennas should allow for spatiotemporal temperature mapping in applications where precise measurement of local temperature is needed in real time. *Published by AIP Publishing*. [http://dx.doi.org/10.1063/1.4954907]

The ability to detect the repeated occurrence, precise spatial location, and severity of temperature in real-time is needed in many areas of medicine,[1–7] structural health monitoring,[8–11] material interfaces,[12–15] and electronic heat management.[16–20] In particular, nanoscale-sensing approaches can offer unparalleled spatial temperature information that is not available through conventional methods. While many promising nanoscale approaches are being explored, currently available organic dyes[21–28] and nanocrystal[29–39] temperature sensors suffer from small dynamic range, stochastic blinking phenomena (i.e., fluctuating intensities), and/or photobleaching, limiting the ability to continuously and quantitatively measure temperatures. In order to advance dynamic studies of temperature, new temperature sensors that are simultaneously capable of nanometer spatial resolution and stability over a broad temperature range are needed.

Here, we propose and theoretically demonstrate that thermal expansion differences in a mechano-optical nano-antenna will reversibly alter its structure (conceptual schematics shown in Figures 1(b), 1(c), and 1(e)) and plasmonic resonance (illustrated conceptually in Figure 1(d)) over a broad temperature range. Unlike conventional contact-based microthermocouples,[40–43] mechano-optical nano-antennas are non-contact and therefore allow for far field optical imaging. In this paper, we systematically vary the nano-antenna geometry in order to realize a relationship between optical properties, mechanical displacement, and temperature. Additionally, our theoretical studies show a matching condition of material properties (Young's Modulus) in order to obtain a maximum optical response. Mechano-optical nano-antennas should enable spatiotemporal mapping of local temperature useful in various fields ranging from biomedical to electronic heat managing applications.

With the purpose of introducing the concept and design guidelines for mechano-optical nano-antenna temperature sensing and actuation, our study consists of three components: conceptual verification, antenna structural design, and antenna material design. For conceptual verification of the mechano-optical temperature sensing, establishing a clear and quantifiable definition of the nano-antenna is critical. The schematic and definition of our proposed nano-antenna is illustrated in Figure 2(a). The nano-antenna is composed of two layers of materials with different coefficients of thermal expansion (α_1 and α_2 as shown in Figure 1(e)). The beam length l is the longitudinal length of the antenna. The thickness ratio is defined to be the ratio of thicknesses between the first layer and second layer (d_1/d_2). The radius of curvature (R_c) is conceptually defined to be the radius of a fitted circle to the curved nano-antenna surface. To numerically calculate R_c, the Timoshenko formula (shown as Equation (1) in the supplementary material[46]) was used. In the absence of temperature elevation, the nano-antenna maintains a linear structure, showing an R_c of infinity. Under elevated temperature, R_c then becomes finite. Using this quantifiable definition of the nano-antenna geometry, a series of configurations were simulated to obtain their absorption spectra under temperature elevation.

In order to confirm that mechanical displacement is related to optical change, materials with different coefficients of thermal expansion were used in the simulation to generate different amount of mechanical deformation. We reasoned that a larger difference between coefficients of thermal expansion (i.e., a coefficient of thermal expansion ratio (α_1/α_2) deviates from 1.00) would lead to a larger wavelength shift ($\Delta\lambda$). Five different nano-antenna material configurations were simulated whose parameters, including coefficient of α_1/α_2, R_c, and $\Delta\lambda$, are shown in a table in Figure 2(b). The five different configurations were distinguished by their α_1/α_2 value and compared by their R_c and $\Delta\lambda$. The relative $\Delta\lambda$ was used instead of absolute λ in order to uniformly compare different material compositions. Figure 2(b) shows that a larger mechanical displacement (R_c) of the nano-antenna leads to a larger wavelength shift ($\Delta\lambda$). For the material combination of Au/polymer, the polymer has a large negative thermal expansion coefficient (-1000.0×10^{-6} K^{-1}). This

a)Author to whom correspondence should be addressed. Electronic mail: sleee@umich.edu. Tel.: (734) 764-7054.

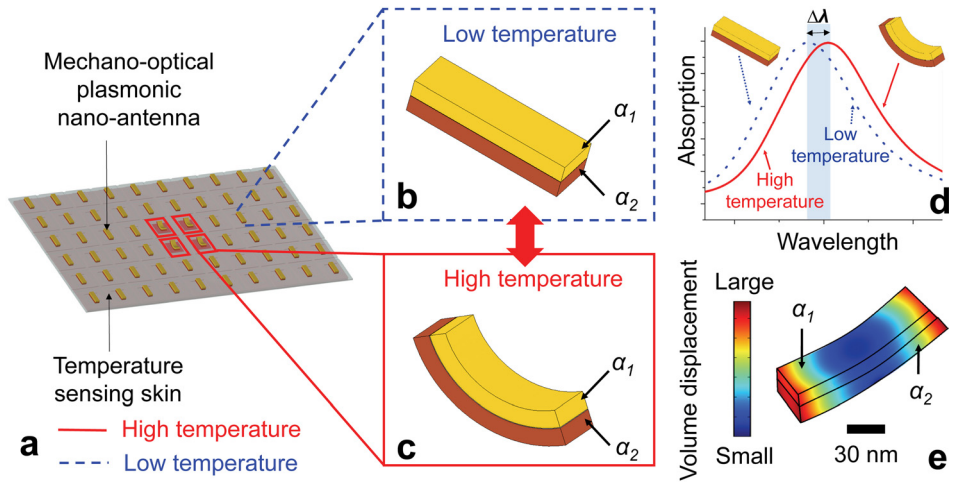

FIG. 1. Concept of mechano-optical plasmonic nano-antenna for temperature mapping. (a) Plasmonic nano-antennas can be used in applications, such as flexible sensing skins, where high spatiotemporal resolution of temperature measurement is needed. (b) Nano-antenna at ambient temperature (no bending). (c) Nano-antenna at elevated temperature (bending). (d) Optical: Localized surface plasmon resonance of the nano-antenna shifts as a result of temperature-induced mechanical displacement. (e) Mechanical: Nano-antenna undergoes mechanical displacement at an elevated temperature due to the difference between the coefficients of thermal expansion (α_1 and α_2); red color indicates more volume displacement, and blue indicates less displacement.

value was taken to be close to that of the state-of-the-art materials demonstrated.[44] All of the configurations show a clear relationship between mechanical displacement and wavelength shift. As a control, Au/Ni was simulated to verify that a minute difference in the coefficients of thermal expansion between Au and Ni rendered minimal mechanical deformation, and thus, no optical change was observed. To closely examine the mechano-optical sensing and actuation, the absorption spectra for the Au/polymer configuration at various radii of curvature, values ranging from 45 nm to infinity, was simulated and shown in Figure 2(c). Upon temperature elevation and increased mechanical displacement, a significant redshift (shown in Figure 2(c) inset as λ_1 and λ_2) of the optical spectrum was observed. The redshift upon structural change is likely due to the deformation of the structure, effectively changing the localized surface plasmon resonance frequency and the coupling between two ends of the nano-antenna upon bending. Therefore, this redshift gets more significant as the temperature increases once the coupling has been established. Additionally, a decrease in absorption intensity was also observed in Figure 2(c). It is likely that this is associated with a decrease in absorption cross-section due to the attenuation of the electric dipole moment[45] when the two ends of the antenna approach each other.

With the above theoretical study verifying our mechano-optical nano-antenna concept, we further investigated the structural design parameters by simulation to achieve optimal device performance. Structural design of the nano-antenna

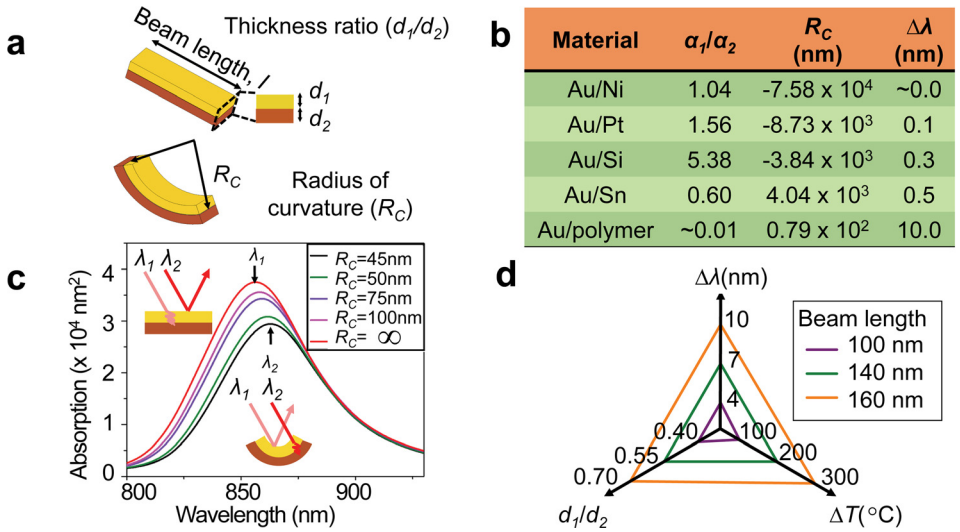

Material	α_1/α_2	R_C (nm)	$\Delta\lambda$ (nm)
Au/Ni	1.04	-7.58 x 10^4	~0.0
Au/Pt	1.56	-8.73 x 10^3	0.1
Au/Si	5.38	-3.84 x 10^3	0.3
Au/Sn	0.60	4.04 x 10^3	0.5
Au/polymer	~0.01	0.79 x 10^2	10.0

FIG. 2. Tuning of the nano-antenna geometry and composition allows for temperature-dependent optical properties. (a) Schematic of the mechano-optical nano-antenna and its geometric parameters. The thickness ratio (d_1/d_2) is defined between the first and the second material thicknesses. The radius of curvature of the nano-antenna is defined to be the radius of a fitted circle to the curved nano-antenna surface (at the interface between the two layers). (b) Comparison table of material type, coefficient of thermal expansion ratio (α_1/α_2), radius of curvature (R_c), and wavelength shift ($\Delta\lambda$). The $\Delta\lambda$ for Au/Sn was obtained with an elevation of 200 °C (close to the melting temperature of Sn), and the $\Delta\lambda$ for all other material configurations were obtained with a temperature elevation of 300 °C above room temperature. The dimensions of the nano-antenna are 160 nm × 30 nm × 17 nm. (c) Calculated absorption spectra as a function of R_c of the nano-antenna. Figure insets illustrate the red-shift upon mechanical deformation. (d) Calculated radar chart of nano-antenna wavelength shift at various temperatures upon tuning the thickness ratio and antenna length.

refers to the shape, dimension, and geometrical structure of the device. As shown in Figure 2(a), the bilayer nano-antenna design offers a significant mechanical displacement while remaining compatibility with current micro- and nano-fabrication. Based on these considerations, we selected the bilayer geometry in this study. Additionally, quantifying the mechanical displacement by R_c ensures a unified measurement standard. With this quantifiable definition, antenna configurations with different lengths, widths, and material compositions can be compared. Therefore, for the structural design of our nano-antenna, we focused on two important geometrical parameters, namely, the beam length l and thickness ratio d_1/d_2, and simulated the effects of these parameters using the Au/polymer configuration (Figure 2(d)). Notably, in Figure 2(d), a larger l and a larger d_1/d_2 (up to approximately 0.7) resulted in a more significant $\Delta\lambda$. A similar increase in $\Delta\lambda$ can also be observed as temperature increases (i.e., higher temperature corresponds to larger wavelength shift of the optical spectrum of the nano-antenna). Since l determines the initial optical spectrum peak position, the target wavelength range should be determined based on application. For best performance, the d_1/d_2 value depends on the coefficients of thermal expansion of the materials used in the antenna, which should be taken into consideration during device design and fabrication. For example, a d_1/d_2 of 0.7 results in the best device performance of the Au/polymer material configuration. Any d_1/d_2 deviating this value resulted in a decrease in R_c and ultimately smaller $\Delta\lambda$. It is worth noting that this d_1/d_2 value that allows for maximum $\Delta\lambda$ based on simulation is consistent with our theoretical calculation based on the Timoshenko formula (Equation (1) in the supplementary material[46]); therefore, it will be used in the studies presented in this paper.

The simulation regarding the nano-antenna geometry gives several fundamental design guidelines, which leads to the next important question of the influence of material properties on the mechano-optical sensing and actuation and whether the general design guidelines in terms of materials can be established. Based on the result in Figure 2(b), the closer the ratio α_1/α_2 is to 1.00 (for example, in the case of Au/Ni, $\alpha_1/\alpha_2 = 1.04$), the smaller the $\Delta\lambda$. Therefore, the Au/polymer configuration gives the largest mechanical displacement as well as the largest optical spectral change. The absolute difference between α_1 and α_2 plays a key role in the mechanical displacement of the antenna. In Figure 1(b), assuming α_1 is a positive value, to achieve a significant $\Delta\lambda$, α_2 should be either a very large positive number (e.g., $\geq 500.0 \times 10^{-6}$ K^{-1}) or a very large negative number (e.g., $\leq -500.0 \times 10^{-6}$ K^{-1}). The specific coefficient of thermal expansion for each material used in Figure 2(b) are listed in supplementary material[46] Figure s1, from which we can see that in the case of Au/Sn, the first layer has a coefficient of 14.2×10^{-6} K^{-1} and the second layer has the largest positive coefficient of thermal expansion of 23.0×10^{-6} K^{-1} among all simulated materials; however, the resulting $\Delta\lambda$ is not significant, which means materials with a larger coefficient of thermal expansion are required to replace the Sn layer. Such materials with large positive coefficient of thermal expansion might be difficult to obtain. On the other hand, large negative coefficients of thermal expansion ($\leq -500.0 \times 10^{-6}$ K^{-1}) have been demonstrated for polymer materials, which should be considered for nano-antenna material selection.

In addition to the coefficient of thermal expansion, Young's modulus of a material also plays a key role in device performance. To theoretically study the effect of Young's modulus, forty different material configurations were simulated, among which the Young's moduli and coefficients of thermal expansion of four representative configurations are listed in the table shown in Figure 3(a). (Figure s2 provides a complete list of material properties for all forty configurations.[46]) The purpose of these four configurations was to compare and illustrate representative nano-antenna performance with and without a Young's moduli mismatch. Material 1 (α_1 and E_1) is composed of various metallic materials, including magnesium (Mg), aluminum (Al), gold (Au), nickel (Ni), and tungsten (W). Material 2 (α_2 and E_2) represents the polymeric material with the coefficient of thermal expansion (α) close to 1000.0×10^{-6} K^{-1}. Since $\Delta\lambda$ is also affected by the difference in α_1 and α_2, the $\Delta\lambda$ was calibrated by changing the coefficient of thermal expansion of the polymer layer so that the difference between α_1 and α_2 remains constant for all metals. To visualize the effect of this mismatch, an interpolation map of Young's moduli (x-axis as E_1 and y-axis as E_2) and wavelength shifts (color bar as $\Delta\lambda$) was created (Figure 3(b); see supplementary material, Figure s2a, for the 40 configurations used to complete the interpolation[46]). It was observed from the interpolation map that the nano-antenna achieved a smaller $\Delta\lambda$ if there was a significant

a

	Material 1		Material 2	
	α_1 (10^{-6} K^{-1})	E_1 (Gpa)	α_2 (10^{-6} K^{-1})	E_2 (Gpa)
i	13.0	170	998.0	600
ii	13.0	170	998.0	200
iii	4.3	411	979.3	50
iv	22.2	69	997.2	800

b

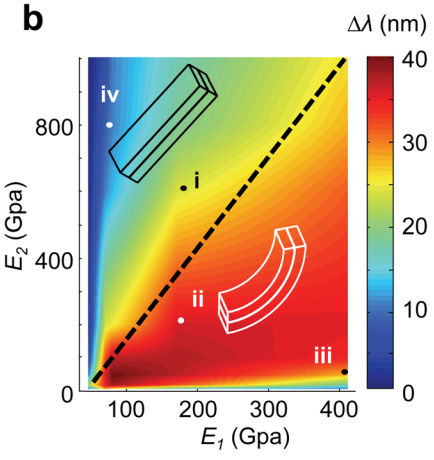

FIG. 3. Mechano-optical actuation requires a matching of Young's Moduli between multi-materials of the nano-antenna. (a) Comparison table of material properties (α_1, α_2) and mechanical properties (Young's moduli E_1, E_2) of four representative nano-antenna configurations. (b) Calculated 2-D interpolation map of $\Delta\lambda$ and E_1, E_2 for nano-antennas at an elevation of 300 °C above room temperature. Representative nano-antennas (i through iv in the comparison table) are displayed on the correlation map with overlaid conceptual schematics. Configurations ii and iv show two distinct mechanical displacements.

Young's moduli mismatch between the two materials. On the map, there also exists a high $\Delta\lambda$ region (red) where the $\Delta\lambda$ is significantly higher than other regions (blue). The $\Delta\lambda$ is less significant when the ratio between the Young's moduli of the two materials becomes too large (e.g., >5). Interestingly, this high $\Delta\lambda$ region (red) is asymmetric with respect to the two axes, as the region tends to be closer to E_1 than E_2. After further investigation, it was determined that the difference in layer thickness (0.7 in this case) caused this asymmetry of the high $\Delta\lambda$ region (red). As a result, the high $\Delta\lambda$ region (red) always tends to shift toward the thinner material layer. Now the nano-antenna design is presented with an interesting consequence: after deciding on the materials based on the difference between α_1 and α_2, an ideal value of d_1/d_2 can be calculated. This d_1/d_2 value then in turn affects the ultimate $\Delta\lambda$ of the device by shifting the high $\Delta\lambda$ region (red). This demonstrates that the thickness ratio serves as a linker between the antenna's mechanical and optical properties. It is also worth noting that the effect of Young's modulus on the wavelength shift can be more significant than the coefficient of thermal expansion. This indicates that the future nano-antenna material selection should entail listing out all possible candidates based on requirements of the application, calculating the position of the high $\Delta\lambda$ region, filtering materials based on their Young's moduli, and finally narrowing down candidates according to their coefficients of thermal expansion.

In conclusion, our theoretical studies revealed the connection between the nano-antenna geometry, material composition, and optical properties in response to temperature, showing that geometrical configuration serves as a linker between the antenna's mechanical and optical properties. Based on these findings, guidelines regarding both material and structural design were proposed. We believe that these guidelines will facilitate the future design of probes for spatiotemporal mapping of temperature useful across various fields, ranging from medicine to heat management.

This work was supported by the National Science Foundation (NSF 1454188) and the Air Force Office of Scientific Research (AFOSR FA9550-16-1-0272).

[1]S. E. Lee, G. L. Liu, F. Kim, and L. P. Lee, Nano Lett. **9**, 562 (2009).
[2]J. N. Anker, W. P. Hall, O. Lyandres, N. C. Shah, J. Zhao, and R. P. Van Duyne, Nat. Mater. **7**, 442 (2008).
[3]K. Riehemann, S. W. Schneider, T. A. Luger, B. Godin, M. Ferrari, and H. Fuchs, Angew. Chem., Int. Ed. **48**, 872 (2009).
[4]D. Le Bihan, J. Delannoy, and R. L. Levin, Radiology **171**, 853 (1989).
[5]L. R. Hirsch, R. J. Stafford, J. A. Bankson, S. R. Sershen, B. Rivera, R. E. Price, J. D. Hazle, N. J. Halas, and J. L. West, Proc. Natl. Acad. Sci. U.S.A. **100**, 13549 (2003).
[6]X. Huang, I. H. El-Sayed, W. Qian, and M. A. El-Sayed, J. Am. Chem. Soc. **128**, 2115 (2006).
[7]H. Xu, I. S. Ramsey, S. A. Kotecha, M. M. Moran, J. A. Chong, D. Lawson, P. Ge, J. Lilly, I. Silos-Santiago, Y. Xie, P. S. DiStefano, R. Curtis, and D. E. Clapham, Nature **418**, 181 (2002).
[8]P. C. Chang, A. Flatau, and S. C. Liu, Struct. Health Monit. **2**, 257 (2003).
[9]I. Kang, M. J. Schulz, J. H. Kim, V. Shanov, and D. Shi, Smart Mater. Struct. **15**, 737 (2006).
[10]M. H. G. Wichmann, J. Sumfleth, F. H. Gojny, M. Quaresimin, B. Fiedler, and K. Schulte, Eng. Fract. Mech. **73**, 2346 (2006).
[11]W. Ecke, I. Latka, R. Willsch, A. Reutlinger, and R. Graue, Meas. Sci. Technol. **12**, 974 (2001).
[12]D. G. Cahill, W. K. Ford, K. E. Goodson, G. D. Mahan, A. Majumdar, H. J. Maris, R. Merlin, and S. R. Phillpot, J. Appl. Phys. **93**, 793 (2003).
[13]M. L. Roukes, K. Schwab, E. A. Henriksen, and J. M. Worlock, Nature **404**, 974 (2000).
[14]C. A. Paddock and G. L. Eesley, J. Appl. Phys. **60**, 285 (1986).
[15]A. Kahn, N. Koch, and W. Gao, J. Polym. Sci., Part B: Polym. Phys. **41**, 2529 (2003).
[16]G. Tessier, M. Bardoux, C. Boué, C. Filloy, and D. Fournier, Appl. Phys. Lett. **90**, 171112 (2007).
[17]M. Mecklenburg, W. A. Hubbard, E. R. White, R. Dhall, S. B. Cronin, S. Aloni, and B. C. Regan, Science **347**, 629 (2015).
[18]L. Aigouy, G. Tessier, M. Mortier, and B. Charlot, Appl. Phys. Lett. **87**, 184105 (2005).
[19]C. C. Williams and H. K. Wickramasinghe, Microelectron. Eng. **5**, 509 (1986).
[20]D. G. Cahill, K. E. Goodson, and A. Majumdar, J. Heat Transfer **124**, 223 (2002).
[21]Z. Wang, X. Ma, S. Zong, Y. Wang, H. Chen, and Y. Cui, Talanta **131**, 259 (2015).
[22]F. H. C. Wong, D. S. Banks, A. Abu-Arish, and C. Fradin, J. Am. Chem. Soc. **129**, 10302 (2007).
[23]O. Yarimaga, S. Lee, D.-Y. Ham, J.-M. Choi, S. G. Kwon, M. Im, S. Kim, J.-M. Kim, and Y.-K. Choi, Macromol. Chem. Phys. **212**, 1211 (2011).
[24]Y. Cui, H. Xu, Y. Yue, Z. Guo, J. Yu, Z. Chen, J. Gao, Y. Yang, G. Qian, and B. Chen, J. Am. Chem. Soc. **134**, 3979 (2012).
[25]J. S. Donner, S. A. Thompson, M. P. Kreuzer, G. Baffou, and R. Quidant, Nano Lett. **12**, 2107 (2012).
[26]K. Okabe, N. Inada, C. Gota, Y. Harada, T. Funatsu, and S. Uchiyama, Nat. Commun. **3**, 705 (2012).
[27]G. Ke, C. Wang, Y. Ge, N. Zheng, Z. Zhu, and C. J. Yang, J. Am. Chem. Soc. **134**, 18908 (2012).
[28]Y. Takei, S. Arai, A. Murata, M. Takabayashi, K. Oyama, S. Ishiwata, S. Takeoka, and M. Suzuki, ACS Nano **8**, 198 (2014).
[29]M. L. Debasu, D. Ananias, I. Pastoriza-Santos, L. M. Liz-Marzán, J. Rocha, and L. D. Carlos, Adv. Mater. **25**, 4868 (2013).
[30]U. Rocha, C. J. da Silva, W. F. Silva, I. Guedes, A. Benayas, A. Elias, E. Bovero, F. C. J. M. Van Veggel, L. M. Maestro, G. S. Jose Antonio, and D. Jaque, ACS Nano **7**, 1188 (2013).
[31]J. Lee, A. O. Govorov, and N. A. Kotov, Angew. Chem., Int. Ed. **117**, 7605 (2005).
[32]L. M. Maestro, E. M. Rodríguez, F. S. Rodríguez, M. C. I. la Cruz, A. Juarranz, R. Naccache, F. Vetrone, D. Jaque, J. A. Capobianco, and J. G. Solé, Nano Lett. **10**, 5109 (2010).
[33]J. Yang, H. Yang, and L. Lin, ACS Nano **5**, 5067 (2011).
[34]E. J. McLaurin, V. A. Vlaskin, and D. R. Gamelin, J. Am. Chem. Soc. **133**, 14978 (2011).
[35]A. E. Albers, E. M. Chan, P. M. McBride, C. M. Ajo-Franklin, B. E. Cohen, and B. A. Helms, J. Am. Chem. Soc. **134**, 9565 (2012).
[36]G. Kucsko, P. C. Maurer, N. Y. Yao, M. Kubo, H. J. Noh, P. K. Lo, H. Park, and M. D. Lukin, Nature **500**, 54 (2013).
[37]T. Plakhotnik, M. W. Doherty, J. H. Cole, R. Chapman, and N. B. Manson, Nano Lett. **14**, 4989 (2014).
[38]S. K. Gordeev and S. B. Korchagina, J. Superhard Mater. **29**, 124 (2007).
[39]J. Tisler, G. Balasubramanian, B. Naydenov, R. Kolesov, B. Grotz, R. Reuter, J. P. Boudou, P. A. Curmi, M. Sennour, A. Thorel, M. Börsch, K. Aulenbacher, R. Erdmann, P. R. Hemmer, F. Jelezko, and J. Wrachtrup, ACS Nano **3**, 1959 (2009).
[40]C. Wang, R. Xu, W. Tian, X. Jiang, Z. Cui, M. Wang, H. Sun, K. Fang, and N. Gu, Cell Res. **21**, 1517 (2011).
[41]X. Zhang, H. Choi, A. Datta, and X. Li, J. Micromech. Microeng. **16**, 900 (2006).
[42]C. Mazieres, Anal. Chem. **36**, 602 (1964).
[43]N. Kawamoto, M.-S. Wang, X. Wei, D.-M. Tang, Y. Murakami, D. Shindo, M. Mitome, and D. Golberg, Nanotechnology **22**, 485707 (2011).
[44]X. Shen, C. Viney, E. R. Johnson, C. Wang, and J. Q. Lu, Nat. Chem. **5**, 1035 (2013).
[45]A. Pors, M. Willatzen, O. Albrektsen, and S. I. Bozhevolnyi, J. Opt. Soc. Am. B **27**, 1680 (2010).
[46]See supplementary material at http://dx.doi.org/10.1063/1.4954907 for detailed simulation parameters and supplementary figures.